Phenothiazine: An Effective Molecular Adhesive for Protein Immobilization

Hsiang Ying Huang and Chong Mou Wang*

Department of Chemistry, National Taiwan Normal University, Taipei 116, Taiwan

Received: October 16, 2009

Protein immobilization is imperative for bioengineering and biochemical applications. Although many excellent approaches have been proposed, most require elaborate skills and labor-intensive techniques. In this work, we report that phenothiazine compounds such as thionine chloride (TC) are potential molecular adhesives for protein immobilization. According to conductive-mode atomic force microscopic analysis (C-AFM), TC exists with a specific affinity for proteins and can be modified on solid surfaces like ITO glass squares (denoted ITO|TC) via a simple diazotization-reduction process. Because the affinity is ∼200 nN, equivalent to 10^2 C−C single bonds, a variety of proteins including glucose oxidase (GOx), glucose dehydrogenase (GDH), ferritin (FT), bovine serum albumin (BSA), and salmon testes DNA (DNA) can thus be immobilized on ITO through TC. Most proteins, however, behave like insulators in aqueous solutions (0.1 M KCl). For this reason, the protein-treated ITO|TC electrodes exhibited insignificant electric responses to the applied bias voltage (V_s) until $|V_s| > 1$ V, contrasting sharply with the current−voltage curves found with bare ITO and ITO|TC. According to the Simmons model for metal|insulator|metal junctions, we estimated the energy barrier (Φ_B) to the transport of electrons in proteins to be 1.0−1.5 eV, and the effective mass of the electrons (m^*), to be 1/1000 the mass of free electrons. We also noticed that FT showed similar results on Φ_B and m^* as adsorbed on ITO|TC and ITO. TC is thus suggested not to interfere with the charge transport in the attracted proteins. Some other phenothiazine compounds were also characterized for their potential as molecular adhesives. Although their performances were not as promising as that of TC, phenothiazine compounds prove to be useful molecular glues for protein immobilization.

Introduction

Electron tunneling exists in biochemical reactions where the interaction between electron donor (D) and acceptor (A) is weak.[1] Although direct measurement of electron tunneling between D and A is challenging, it is conceptually possible to picture the tunneling current by mimicking D and A with electron reservoirs such as electrodes. A stationary current would flow through the system in this case with an amplitude that is a function of the thickness and the energetics of the spacer relative to the electrodes.[2,3]

Through billions of years of evolution, biological entities, such as proteins, have been perfected structurally and functionally to cope with photo-, electrical, and chemical stimuli. Proteins are known to perform a wealth of functions, including energy conversion, transportation, and information processing. To gain a deeper insight into the biological codes controlling electron transport in proteins as well as to develop molecular electronics[4] for biosensing[5] and immunoassay,[6] biocircuitry that integrates proteins into nanotechnology has been developed to be an effective means besides many other approaches, such as biochemical assays,[7] time-resolved spectroscopic measurements,[8] electrochemical analysis,[9] and single-molecule spectroscopy.[10] Conductance measurements are also effective in this aspect.[11] However, experimental observations seemed to be in dissonance; for instance, a debate has been raised over the ability of DNA to transport charge and the nature of the conduction mechanisms through it.[12] Most conflicts appear to result from the difference in experimental conditions as well as the difficulty in controlling the interaction of biomolecules with solid surfaces and the contacts with the probes. These problems can be overcome by employing a metal-covered atomic force microscope (AFM) tip to pass current through biomolecules that are chemically connected to a metal substrate at one end and to a gold nanoparticle at the opposite end.[13] Many biochemical devices have benefited from this idea,[14−18] showing promise in a variety of applications.[6,19,20]

Regarding protein attachment, many excellent approaches have been reviewed, including physical adsorption, electrostatic attraction, specific recognition, and covalent binding.[20] These methods have demonstrated application potential in many areas; however, most require elaborate techniques and skills. Simple and effective molecular adhesives[21] that can stick to proteins or induce their homo- or heterotropic assembly have become imperative in bioengineering as well as in the understanding of the charge-transport properties of protein. In this work, we demonstrate that phenothiazine compounds, such as thionine chloride (TC), are potential molecular adhesives that can be applied to most proteins and electrode surfaces. When TC was modified on indium−tin oxide (ITO) conductive glass via a diazotization-electrochemical reduction process,[22] the resultant surface showed a strong affinity for proteins, including oxidase, dehydrogenase, iron-storage protein, and DNA. The binding strength was estimated to be ∼200 nN, equivalent to 10^2 C−C single bonds, more significant than that for ITO (>30 nN).[22] Despite the affinity being significant, the glue showed negligible interference with the proteins in charge transport. Phenothiazine compounds thus prove to be simple and effective molecular adhesives for protein immobilization.

Experimental Section

Materials. Toluidine blue O, methylene blue, and thionine chloride were purchased from Aldrich and used as received

* To whom correspondence should be addressed.

10.1021/jp9119099
Published on Web 02/09/2010

SCHEME 1: Electrode Modifications of ITO with TC and Proteins

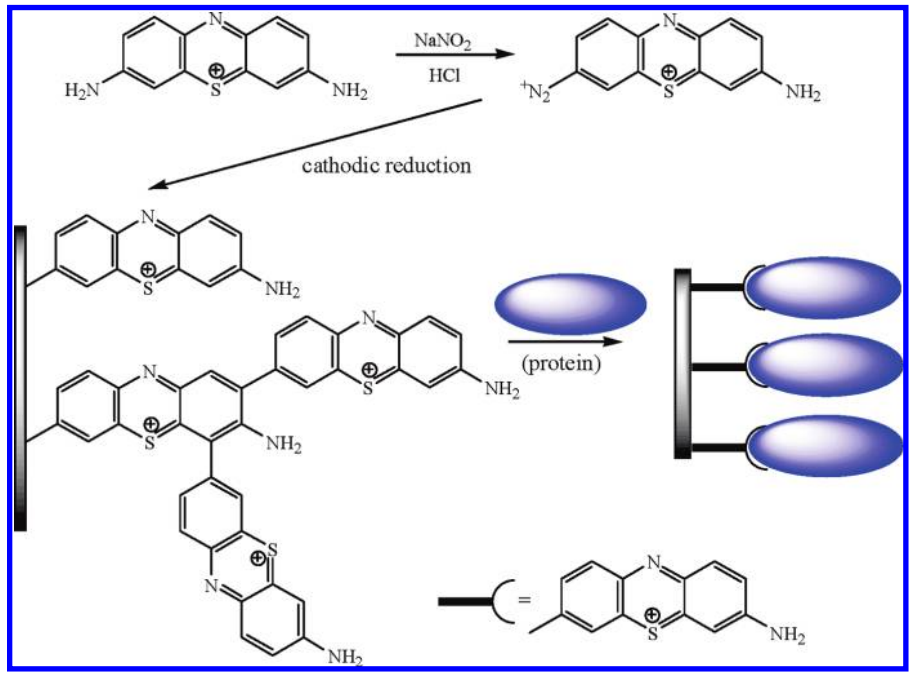

without further purification. $NaNO_2$ was supplied by Merck. GOx, GDH, BSA, FT, and DNA were obtained from Sigma. ITO glass squares (indium-doped, 0.7 mm thick, 20 Ω cm^{-2}) were supplied by Delta Technologies.

Surface Modifications. Unless otherwise mentioned, TC and proteins were modified on conductive ITO glass squares (0.5 × 0.5 cm^2). The glass squares were thoroughly cleaned according to the procedure described elsewhere to remove all the possible organic and inorganic contaminants before surface modifications.[22] TC modification was carried out via a diazotization-reduction approach. Typically, TC (20 mM) was first mixed with equimolar $NaNO_2$ in 0.1 M HCl, and then, subjected to an immediate potential cycling from 0 to −0.6 V vs SCE for 10 cycles at a constant scan rate (20 mV/s) using the ITO square as the working electrode. The resultant ITO squares (denoted ITO|TC) were then soaked in solutions containing desired proteins for 4 h. The resultant electrodes (ITO|TC|protein) were subsequently characterized in 0.1 M KCl with cyclic voltammetric techniques (CV) to ensure that TC and protein had been deposited firmly on the ITO substrates.

Apparatus. A PAR 283 potentiostat (EG & G) was used for electrode modifications and characterizations. Unless otherwise specified, all experiments were carried out in a nitrogen environment in a one-compartment cell with a Pt counter electrode and an SCE reference electrode. Atomic force microscopic (AFM) images and current−voltage data were recorded on a Nanoscope III E AFM (Digital Instruments, Santa Barbara) operating in tapping, contact, and conductive modes. For surface scratching measurements, we first scanned samples with tapping-mode AFM and obtained the topographic image and then scratched the surface in contact mode. The height profile across the scratch on the film gave the film thickness. For conductive mode imaging (C-AFM), a home-built preamplifier, with a sensitivity of 1 nA/V and operational range from 1 pA to 10 nA, was used for current measurements. The AFM tip and cantilever were coated with a 15 nm Pt layer. The force constant of the cantilever was regularly calibrated against calibrated cantilevers. Force and current vs displacement curves were obtained with speeds of approach between 60 and 2900 nm/s on protein coated surfaces. The conductive tip behaved effectively as a metal electrode with an area mainly determined by the tip−sample contact region. With the tip at virtual ground, a selectable bias voltage was applied between the tip and sample. In the C-AFM analysis, the rms noise level was about 2 pA and any signal above this value was detectable. The deflection of the cantilever was monitored and kept constant to maintain a constant force between the tip and sample, and simultaneous topographic and current images were generated. After every current−voltage measurement, we scanned the same region of the film to ensure that the current−voltage data were valid, rather than coming from surface damage. Humidity was controlled by a humidity controller in conjunction with a homemade N_2/H_2O flow system.

Results and Discussion

Thionine chloride (TC) is a potential molecular adhesive for proteins. When TC was modified on ITO electrodes via a simple diazotization-reduction process as illustrated in Scheme 1, the electrode roughness increased from 10 to 40 nm, and even to 70 nm after the resultant electrode (denoted ITO|TC) was soaked in a solution containing glucose oxidase (GOx, 3 mg/mL, pH 7 phosphate buffer; Supporting Information, Figure S1). The alterations in this aspect are similar to the reports on GOx as adsorbed on silicon oxide and other substrates.[23−25] By contrast, when TC was excluded initially, only insignificant variations could be observed.

Conductive AFM image analysis (C-AFM, Figure 1) confirms the affinity of TC for proteins. As ITO|TC was treated with GDH, the protein molecules (greenish-yellow dots, ∼20 nm) were attracted to stick on the TC sites (blue), similar to GOx and ferritin (FT) on ITO|TC (Supporting Information, Figure S2). Here the TC sites are noticed to be less than 2 nm in size, relatively small compared with the roughness of ITO|TC. The discordance in this aspect suggests that TC, as modified on ITO, might form multiple layers[26] on ITO as proposed in Scheme 1.

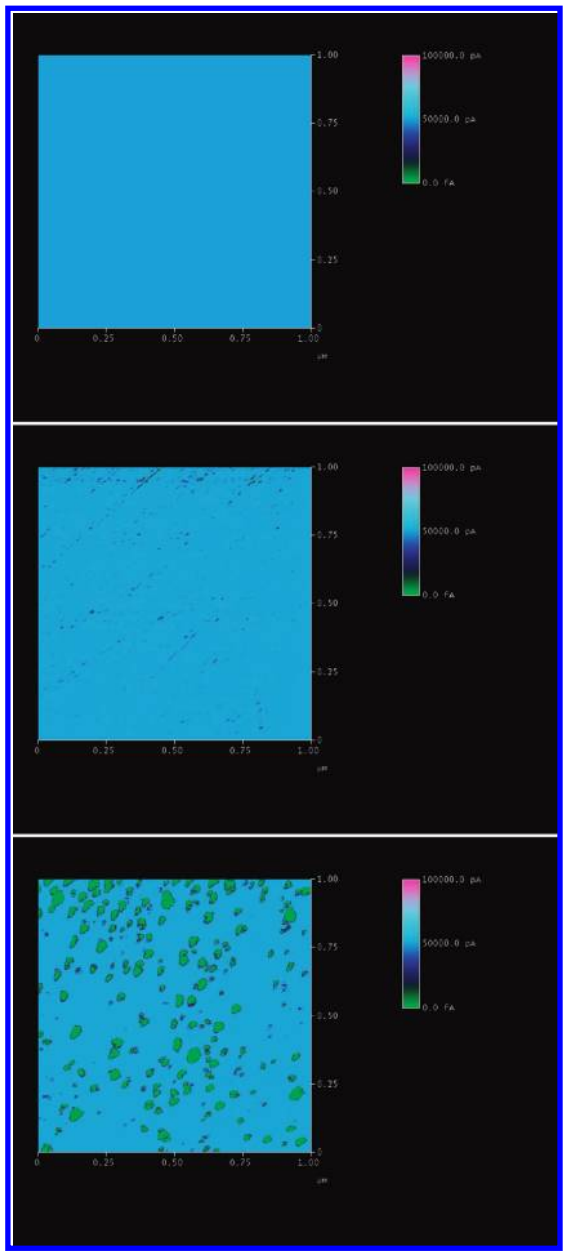

Figure 1. C-AFM images of ITO (upper), ITO|TC, and ITO|TC|GDH (bottom); $V_s = 1$ V.

Prior to the C-AFM imaging, ITO, ITO|TC, and the protein-treated ITO|TC electrodes (denoted ITO|TC|protein) were characterized regarding their responses to an applied bias voltage (denoted V_s; with the tip at virtual ground) in a constant-force mode (5 nN). Figure 2A shows that ITO generally followed Ohm's law before the transmitted currents (I) reached the set values (±32 nA, trace a). The contact resistance was accordingly estimated to be ~5 MΩ. In contrast, ITO|TC revealed nonlinear correlations in this aspect (trace b). Here, the $I-V_s$ curves similar to trace b were recorded over different sites on ITO|TC, corresponding to a probability of ~30%. The low probability is ascribed to imperfect distribution of TC over the electrode surface and damage caused during the C-AFM image scanning. Despite this, the $I-V_s$ curve transformed into a pattern like trace c immediately after ITO|TC was soaked in GDH solutions. The difference between the responses of the electrodes to a given V_s correlate well with the relative conductivities of ITO, TC and GDH ($V_s = 1$ V) reflected in the C-AFM images shown in

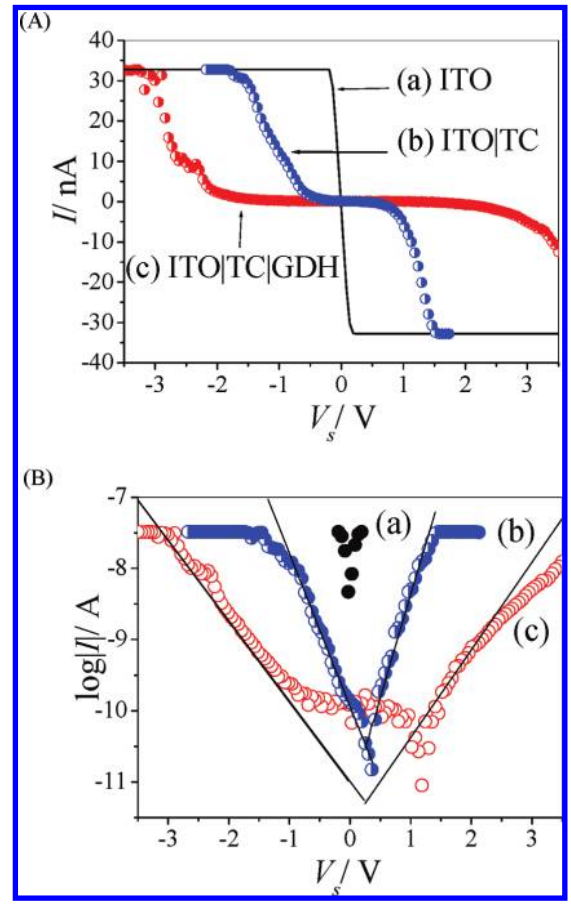

Figure 2. (A) Representative $I-V_s$ curves for (a) ITO, (b) ITO|TC, and (c) ITO|TC|GDH. Panel B shows the corresponding semilog plots.

Figure 1. Substitution of other proteins like GOx and FT for GDH also showed similar results in this respect (Supplementary data: Figure S3). TC is evident to exist with a specific affinity for protein.

On increasing the force load (F_{appl}) to 200 nN, we found that ITO|TC|protein showed no signs of change in their $I-V_s$ curves (in log|I|$-V_s$ representation), contrasting sharply with the responses of bare ITO and ITO|TC to F_{appl} in this respect (for ITO, the contact resistance decreased from 10^8 Ω to 10^6 Ω as F_{appl} increased from 5 nN to 7 nN; for ITO|TC, it decreased from 10^{10} Ω to 10^9 Ω). Typical results are shown in Figure 3A (for ITO|TC|FT) and the Supporting Information (Figure S3, for other ITO|TC|protein). According to these results, the protein molecules adsorbed on ITO|TC appear tougher than the water molecules or TC lying on ITO against the piercing of the AFM tip. On further increasing F_{appl}, the current responses of ITO|TC|FT (and other electrodes as well) started to change, transforming into the curves characteristic of ITO|TC and ITO ($F_{appl} = 0.9$ and 7.4 μN) successively. These changes signal that the protein and TC beneath the tip were being dislocated one after another, causing the TC site and the ITO substrate to contact with the tip. Similar transitioning also occurred on ITO|FT (Figure 3B); however, the pattern is different. The curve characteristic of ITO|TC seen in the case of ITO|TC|FT at 0.9 μN did not appear in the case of ITO|FT; instead, a curve resembling the characteristic of bare ITO was observed. Here ITO|FT was prepared according to a procedure reported in the literature.[27] The difference between the two cases strongly suggests that adsorption of proteins on TC be more favorable than on ITO, consistent with the

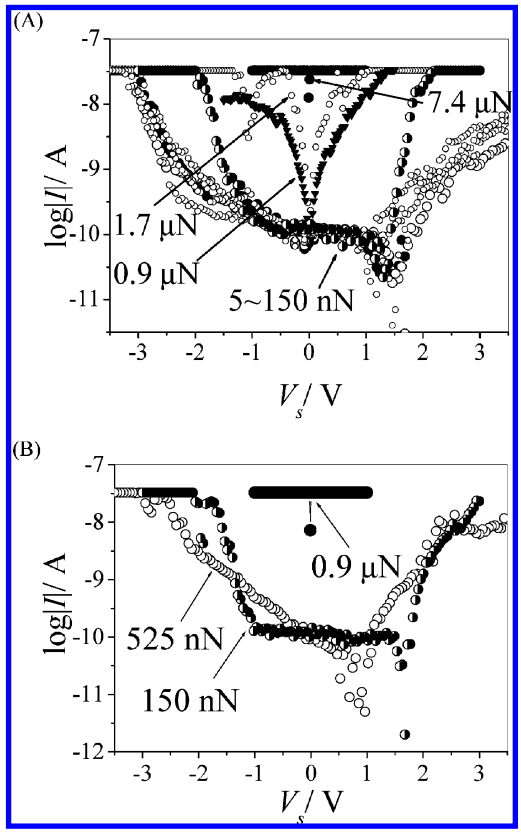

Figure 3. $\log|I|-V_s$ curves of ITO|TC|FT (A) and ITO|FT (B) recorded under varying F_{appl}.

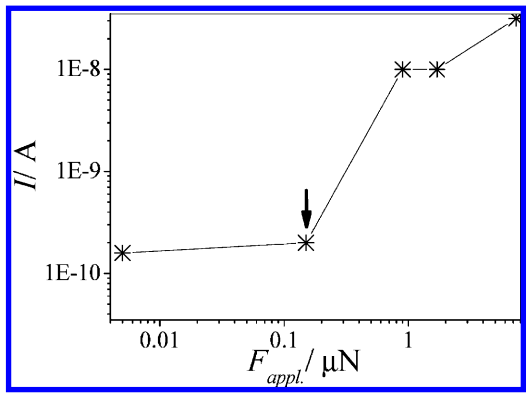

Figure 4. Plots of I versus F_{appl}; the currents were sampled from ITO|TC|FT at $V_s = 1$ V.

preferential adsorption of GDH on TC as shown in Figure 1 (C). The strong affinity is tentatively ascribed to the force of attraction between the positively charged TC layer and the negatively charged proteins (the pI values are 4.3, 4.7, and 4.4 for GOx, BSA and FT, and 4−6, for NADP-dependent GDH).[28,29] Protein molecules with higher pI such as PQQ-dependent GDH (pI = 9.5)[30] were also tested and showed similar affinity for TC. In view of this, some other effects, such as specific interactions through extended π systems[31] and van der Waals force[32] may also contribute to that affinity. Although the origin is not fully identified, according to the turning point marked in the plots of I vs F_{appl} displayed in Figure 4, the strength of the interaction between TC and proteins is estimated to be ~0.2 μN, equivalent to 10^2 C−C single bonds.[33]

Further analysis of the $I-V_s$ curve of ITO|TC (Figure 2A, trace b) revealed a V-shaped characteristic for the surface in terms of log|I| vs V_s (Figure 2B, trace b). The shape, however, became twisted as proteins were incorporated (Figure 2B trace c and Figure S4), leading to $dI/dV_s \approx 0$ within ±1 V. Regarding this alteration, ITO|TC is electrochemically active, displaying a pair of quasi-reversible waves near 0.2 V vs SCE in aqueous KCl (0.1 M), corresponding to $TC^{0/-}$, whereas GDH, GOx, FT, and BSA act like insulators, showing no sign of electron transfer within ±1 V. The difference in this aspect could lead to a state of $I = 0$ when a thin layer of protein is adsorbed on ITO|TC in which the height of the energy gap induced by the protein is positioned above the Fermi levels of ITO|TC and the counter electrode (AFM tip). Taking into consideration this hypothesis and the overvoltage induced by protein molecules, the energy gap should be greater than 1 eV in height, sufficient to block the process $TC^{0/-}$ on ITO|TC.

Two mechanisms might explain the twisted $I-V_s$ curves of ITO|TC|protein: thermionic emission (also known as Schottky emission)[34] and electron tunneling.[3] The former predicts that the transmitted currents tend to limiting values with negative dI/dV_s as V_s approaches ±∞

$$I = \sigma\{[\exp(\eta V_s) - 1]/[\exp(\eta V_s) + 1]\} \quad (1)$$

where σ and η are constants. The prediction, however, contrasts with the observed data, especially, on dI/dV_s. Since ITO|TC|protein|Pt (Pt = Pt-coated AFM tip) shows a similarity to metal|DNA|metal[35,36] in junction characteristic, the electrons flowing across protein might be through tunneling

$$I = (q\Gamma/2\pi hd^2)\{\phi \exp[-4\pi(2m^*)^{1/2}d(\phi)^{1/2}/h] - (\phi + qV_s)\exp[-4\pi(2m^*)^{1/2}d(\phi + qV_s)^{1/2}/h]\} \quad (2)$$

The current depends strongly on the position of the Fermi level of the emitter and collector relative to the HOMO and LUMO of the insulating spacer.[37] Here q is the electron charge; Γ, the effective area for electron transport; h, the Planck constant; d, the effective distance in transport; ϕ, the mean tunnel barrier height; and, m^*, the effective mass of the electron. If the applied bias (V_s) is lower than the barrier height (Φ_B), d and ϕ approximate to the barrier width (L) and ($\Phi_B - qV_s/2$), respectively, leading to the following correlation between I and V_s

$$I = q\Gamma/(2\pi hL^2)\{(\Phi_B - qV_s/2)\exp[-4\pi(2m^*)^{1/2}(\Phi_B - qV_s/2)^{1/2}L/h] - (\Phi_B + qV_s/2)\exp[(-4\pi(2m^*)^{1/2}(\Phi_B + qV_s/2)^{1/2}L/h)]\} \quad (3)$$

As V_s is far smaller than the height (i.e., $|qV_s| \ll \Phi_B$), an exponential correlation between I and V_s results, predicting a V-shaped characteristic for ITO|TC|protein as shown in Figure 2B (trace c) in terms of log|I| versus V_s

$$I \approx I_0\{\exp(\gamma V_s) - \exp(-\gamma V_s)\} \quad (4)$$

$$I_0 = [q\Gamma\Phi_B/(2\pi hL^2)]\exp[-4\pi(2m^*)^{1/2}\Phi_B^{1/2}L/h] \quad (5)$$

Here $\gamma = \pi(2m^*)^{1/2}qL/(\Phi_B^{1/2}h)$. Conversely, if $qV_s \gg \Phi_B$, $d \rightarrow \Phi_B L/qV_s$ and $\phi \rightarrow \Phi_B/2$. Injection tunneling would dominate the whole charge-transport process. The tunneling current turns

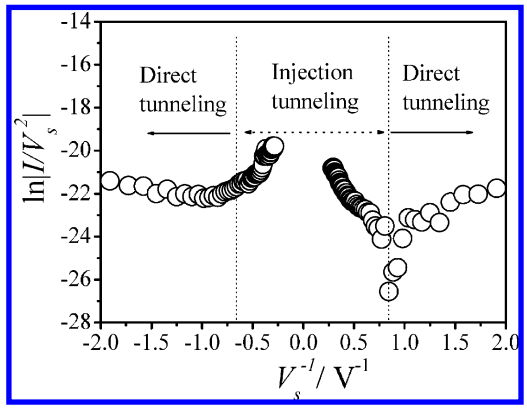

Figure 5. Representative $\ln|I/V_s^2|$ and V_s^{-1} plots for ITO|TC|GDH.

TABLE 1: Φ_B, m^*, and L for GDH, GOx, BSA, Salmon Testes DNA, and FT

protein	Φ_B/eV	m^*/m	L/nm	$\Phi_B(m^*/m)^{1/3}$
GDH	1.26 (1.12)	0.005 (0.005)	10	0.2 (0.18)
GOx	1.39 (1.20)	0.0003 (0.0005)	30	0.08 (0.09)
BSA	1.60 (1.51)	0.006 (0.002)	10	0.3 (0.21)
DNA	1.34 (1.12)	0.015 (0.002)	7[a]	0.3 (0.40)
FT	1.46 (1.27)	0.004 (0.15)	7[a]	0.22 (0.68)
FT[b]	1.33 (1.30)	0.005 (0.15)	7[a]	0.22 (0.68)

[a] Approximated by the roughness of ITO. [b] Estimated from ITO|FT.

out to increase with V_s^2, or more precisely, decreases linearly with the reciprocal of V_s in terms of $\ln(I/V_s^2)$[38]

$$I = \{V_s^2 q^3 \Gamma/[8\pi h L^2(\Phi_B/2)]\} \times \exp[-8\pi(2m^*)^{1/2}(\Phi_B/2)^{3/2}L/hqV_s] \quad (6)$$

As seen in Figure 5, ITO|TC|GDH demonstrates a linear correlation between $\ln(I/V_s^2)$ and V_s^{-1} in the range: $V_s^{-1} < 0.6$ V^{-1} ($V_s > 1.6$ V). Similar results also appeared on the negative voltage side when the corresponding currents were treated in a similar way. In theory, eq 6 does not hold as $|qV_s| \rightarrow \Phi_B$. For this reason, disruption occurred at $|V_s|^{-1} \approx 0.7$ V^{-1}, dividing the plots into two transport regimes: direct tunneling and injection tunneling. The crossover between these two regimes, i.e., $|qV_s| = \Phi_B$, turns out to be an indication of the location of Φ_B. Based on the potential for each crossover point, we estimated the barrier height associated with each protein to be 1.0−1.5 eV. The results are listed in Table 1, agreeing with the overvoltage (the range of potential where $\partial \log|I|/\partial V_s \approx 0$) reflected in each corresponding $\log|I|-V_s$ curve. Using the average Φ_B and assuming L to be the electrode roughness of each protein-modified electrode, we conclude that for most proteins in this work, $\Gamma \approx 0.8$ nm^2 and $m^* \approx 10^{-3}m$ (the mass of a free electron) or $\Phi_B \approx 0.2(m/m^*)^{1/3}$ (Supporting Information, Figure S4), consistent with those reported on protein membranes such as the purple membrane of *Halobacterium salinarum* ($\Phi_B \approx 2$ eV; $m^* \approx 0.04$ m; $\Phi_B \approx 0.68(m/m^*)^{1/3}$; $\Gamma \approx 0.2$ nm^2).[39] It is noteworthy that FT showed similar Φ_B and m^* as adsorbed on ITO|TC (ITO|TC|FT) or on ITO (ITO|FT). TC is thus implied that it would not interfere with the charge transport in proteins. The ITO|TC|protein|Pt junction can therefore be simplified to ITO|protein|Pt, conforming to the Simmons model.[3] Recently, Xu et al. also performed conductivity measurements on FT, concluding that $\Phi_B = 0.19(m/m^*)^{1/3}$ eV for single apoferritin, and $0.097(m/m^*)^{1/3}$ eV for single holoferritin,[17] which is compatible with our findings. We also characterized salmon testes DNA (denoted DNA) for comparison. The resolved m^* is about 10 times smaller than those of single and short DNA molecules.[40,41] The electron tunneling in bulkier DNA is thus concluded to be less efficient than in shorter DNA,[42] tentatively ascribed to the lack of ordered electron-transport channels and/or protein folding.

SCHEME 2: Illustration of the Energy Level Bands[a]

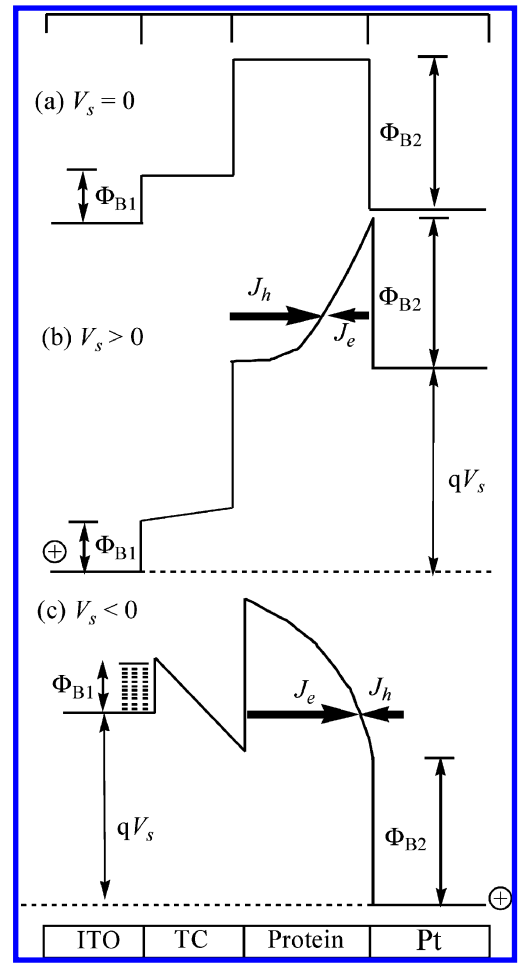

[a] (a) Energy bands between the tip and substrate assuming that the electric field between the tip and substrate is even. (b) If the nonuniformity of the electric field is considered, electrons (holes) tunnel through a narrower (wider) potential barrier than the triangular potential barrier when the tip is negative relative to the substrate; J_e and J_h stands for the fluxes of electrons and holes, respectively. (c) Electrons (holes) tunnel through a wider (narrower) potential barrier than the triangular potential barrier when the tip is positive relative to the substrate.

The $I-V_s$ curves of ITO|TC|protein are not entirely symmetric. Substitution of gold or graphite for ITO showed similar problems in this aspect. Asymmetry in $I-V_s$ curves is a challenge to C-AFM analysis, which might be generated by employing different molecule−electrode contacts on the two ends,[43] by using different electrodes,[44] or by the nonuniformity of the electric field between the tip and the substrate.[17] According to the energy bands illustrated in Scheme 2, the electric field near the top of the tip is larger than the electric field near the ITO substrate, where Φ_{B1} and Φ_{B2} stand for the height of the barriers induced by TC and protein, respectively. If a positive bias is applied to the substrate, such as the case shown in (b), electrons (holes) contributing to the tunneling current would tunnel through a potential barrier narrower (wider) than the case of a negative V_s (case (c)). In our case, the currents

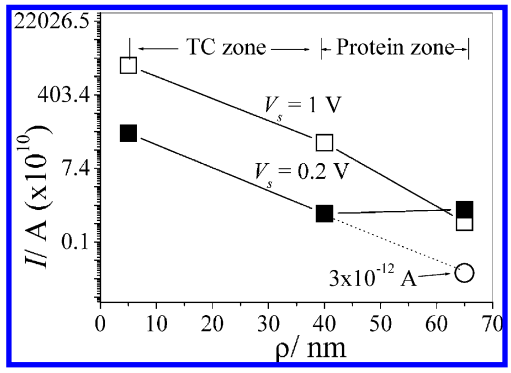

Figure 6. Relationships between I and the roughness (ρ) of ITO, ITO|TC and ITO|TC|GOx. The currents are sampled at 1 V (open square) and 0.2 V (solid square); ○, the predicted value.

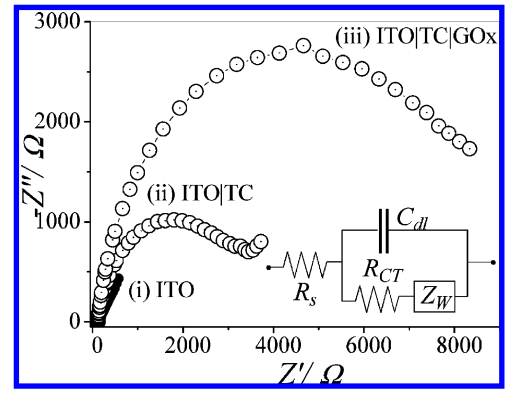

Figure 7. Representative Nyquist plots for (i) ITO, (ii) ITO|TC, and (iii) ITO|TC|GOx recorded in 0.1 M KCl containing 1.5 mM $Ru(NH_3)_6^{3+}$. Inset: the equivalent circuit used for data simulation.

generated from the negative voltage side are greater than those from the positive voltage side. Holes are thus thought to be the dominant carriers in protein. This is consistent with most studies on proteins and explains why the Φ_B determined based on the cathodic currents (Table 1, bracketed) are smaller than those from the anodic counterpart.

The currents transmitted from ITO, ITO|TC, and ITO|TC|protein are not only voltage dependent but also closely related to their surface roughness (ρ). When we plotted the currents of ITO, ITO|TC and ITO|TC|GOx obtained under the conditions: V_s = 1 V and F_{appl} = 5 nN against the ρ associated with each electrode, an exponential correlation appeared as shown in Figure 6, similar to the single-step hole-transport dynamics found with DNA:[40,45]

$$I = I_{max} \exp(-\beta\rho) \quad (7)$$

Here I_{max} and β stand for the effective current and the structure-dependent factor.[46] According to eq 3, if V_s is kept constant and small, the tunneling current turns out to be a function of L

$$I \approx [q\Gamma\Phi_B/(2\pi hL^2)]\{\exp(-\beta L) - \exp(\beta' L)\} \quad (8)$$

where $\beta = 4\pi(2m^*)^{1/2}(\Phi_B - qV_s/2)/(\Phi_B^{1/2}h)$; $\beta' = 4\pi(2m^*)^{1/2}(\Phi_B + qV_s/2)/(\Phi_B^{1/2}h)$. Because the exponential terms in eq 8 converge more quickly with increasing L than the pre-exponential term, the current is expected to follow an exponential decay as described by eq 7. Distance dependence also exists in the case of larger V_s ($|qV_s| > \Phi_B$) according to eq 6. The tunneling current in this case would roughly decrease in a manner with $L^{-2}\exp(-\beta L)$ instead of $\exp(-\beta L)$. Considering these, the electron tunneling in ITO|TC|GOx is apparently not confined on GOx solely; it is likely to extend from GOx to TC. TC thus proves to be not only a potential molecular adhesive but also an effective electric wire for proteins. Based on eq 7, we predicted the current at 0.2 V (where $I \approx 0$) to be 3×10^{-12} A (open circle marked in Figure 6). The predicted values, however, deviate greatly from the measured ($\sim 10^{-10}$ A). We ascribe the discrepancies to the interference from nonfaradaic currents. Nonfaradaic charging can induce charging current (I_c), thereby interfering with the faradaic current as electrodes are subjected to voltage sweeping

$$I_c = \upsilon C_{dl} \quad (9)$$

TABLE 2: Double-Layer Capacitance of ITO|TC|Protein and ITO|FT

sample	C_{dl}/F
ITO|TC|GDH	7.8×10^{-12}
ITO|TC|GOx	7.0×10^{-12}
ITO|TC|BSA	9.8×10^{-12}
ITO|TC|DNA	9.0×10^{-12}
ITO|TC|FT	8.0×10^{-12}
ITO|FT	1.0×10^{-11}

Here C_{dl} and υ stand for the double-layer capacitance of ITO|TC|protein and the rate of potential sweeping. The charging current, or more precisely, the admittance of ITO|TC|protein near the potential where $I = 0$, is less likely to be contributed by ITO or TC, and more likely, by the adsorbed proteins because ITO and ITO|TC showed no signs of charge accumulation according to the associated $\log|I| - V_s$ curves shown in Figure 2B (traces a and b). Assuming the current observed near the potential where zero current is expected to be I_c, we measured I_c for each ITO|TC|protein at different υ and plotted them against υ (the representative plots given in Figure S6). The C_{dl} associated with each protein was estimated to be $\sim 10^{-11}$ F (Table 2), or 10^{-3} F/cm^2 as Γ (=0.8 nm^2) is taken into consideration. The capacity is about 10^6 times that of the molecular junction fabricated by benzene-1,4-dithiol ($\sim 10^{-19}$ F).[47] Proteins thus prove to be potential charge reservoirs. The value of β for GOx was determined to be $\sim$0.02 Å^{-1}, about 40 times less than those for redox enzymes or synthetic DNAs.[46,48] β is a measure of the efficacy of charge transfer within a given space. Charge transport in proteins is thus considered less facile than in DNA, consistent with the values of m^* listed in Table 1.

DNA is a highly organized scaffold and an effective medium for long-distance charge transfer,[49,50] in which nucleobases such as guanine function as charge carriers.[51−53] Unlike DNA, proteins lack $\pi-\pi$ stacked array of nucleic acid base pairs. The charge transport in proteins may thus rely on methionine, tryptophan, tyrosine and/or phenylalanine. Methionine is readily oxidized into methionine sulfoxide via a relay process by which electrons can transfer from the protein surface to a buried methionine.[54]

$$\text{methionine} + H_2O \rightarrow \text{methionine sulfoxide} + 2e^- + 2H^+ \quad (10)$$

Reaction 10, however, is virtually irreversible unless methionine sulfoxide reductase is present.[55] Folding is also a challenge to proteins in charge transfer.[56] Considering these drawbacks and

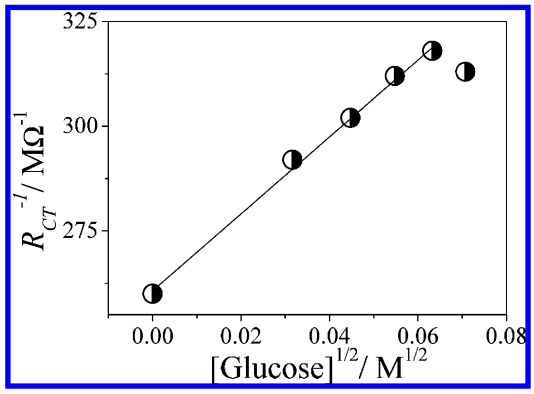

Figure 8. Relationship between the reciprocal of R_{CT} of ITO|TC|GOx and the square root of the concentration of glucose added in oxygenated solutions.

TABLE 3: Kinetic Elements Involved in the Equivalent Circuits Associated with ITO, ITO|TC, and ITO|TC|GOx

	element			
condition	R_s/Ω	C_{dl}/μF	R_{CT}/Ω	Z_W
ITO	109	1.7×10^{-5}	17	0.002
ITO|TC	106	1.0×10^{-5}	1766	0.0004
ITO|TC|GOx	100	1.0×10^{-5}	4717	0.0003

the fact that the amino and carboxyl groups in the sequence and residues of proteins are potential microcapacitors for charges, the current induced by nonfaradic processes on ITO|TC|protein may thus dominate over the faradaic counterpart in the case $|V_s| < \Phi_B/q$.

Impedance analysis of ITO|TC|GOx provides further evidence for the unique property of TC toward proteins. Figure 7 shows that when ITO|TC incorporated GOx, the electrode impedance increased substantially, reflected in the complex plots measured in 0.1 M KCl/1.5 mM $Ru(NH_3)_6^{3+}$ (pH 7). Here, the electrodes were biased at −0.19 V vs SCE, near the formal potential of $Ru(NH_3)_6^{3+/2+}$, superimposed with an ac perturbation (±10 mV) oscillating from 0.1 MHz to 0.1 Hz. Data simulation was carried out based on a simple Randles circuit as inset in Figure 7; the results are listed in Table 3, where R_{CT}, R_s, C_{dl}, and Z_W stand for the charge-transfer resistance, the solution resistance, the double-layer capacitance, and the Warberg impedance. The relative errors in both in-phase and quadrature phase are less than 10%. Equivalent circuits of higher levels, such as circuits adopting three in-series *RC* loops, were also employed for data simulation. This extension reduced the relative errors slightly but not significantly. Data simulations with multiplayer *RC* circuits are thus considered un-necessary for our case, indicating that the GOx and TC on ITO|TC|GOx are likely to stick tightly together as an integrated entity in lieu of two discrete in-series *RC* loops. According to Table 3, R_{CT} increases systematically throughout the electrode modification, whereas C_{dl} remains almost unchanged. The increase in R_{CT} confirms the adsorption of GOx on the electrode. For C_{dl}, the values are ∼10 μF/cm^2, far smaller than the capacitance of GOx (∼10^3 μF/cm^2). Considering that $C_{dl}^{-1} \approx C_{dl,GOx}^{-1} + C_{dl,ITO}^{-1}$, the quadrature component (90°) of the impedance is evidently controlled by the double layer of ITO, i.e., $C_{dl,ITO}$. This result explains the similarity among ITO, ITO|TC, and ITO|TC|GOx in C_{dl}. Besides C_{dl}, we also notice that R_s remains unchanged throughout the electrode modification. Since in impedance measurements, the electrolyte solutions were not perturbed, a constant R_s is thus expected. For Z_W, the values are less significant than those of R_{CT}. Mass transport is thus considered not a challenge to charge transport in our system. Thanks to the strong affinity of TC for GOx, ITO|TC|GOx demonstrated a catalytic effect on the transduction of glucose in oxygenated solutions, leading to a decrease in R_{CT} with an increase in the concentration of glucose, or more precisely, an increase in R_{CT}^{-1} with [glucose]$^{1/2}$ as shown in Figure 8

$$R_{CT}^{-1} = A + B[\text{glucose}]^{1/2} \tag{11}$$

where A and B are constants. Besides R_{CT}, we also noticed that the limiting currents (I_∞) of $Ru(NH_3)_6^{3+/2+}$ increased in a similar manner with [glucose]$^{1/2}$ (Supporting Information, Figure S7; I_∞ were approximated by the currents near −0.3 V).

$$I_\infty = nFA[Ru(NH_3)_6^{3+}](k'D[\text{glucose}])^{1/2} \tag{12}$$

In theory, the R_{CT} of the system is a function of the exchange current (I_0) of $Ru(NH_3)_6^{3+/2+}$

$$R_{CT}^{-1} = n_a F I_0/RT \tag{13}$$

The linear correlation existing between R_{CT}^{-1} or I_∞ and [glucose]$^{1/2}$ signals that glucose can accelerate electrons to transfer through ITO|TC|GOx at a rate reaching its diffusion limit. Since substitution of H_2O_2 for glucose under nitrogen could enhance the limiting current of $Ru(NH_3)_6^{3+/2+}$ as well, the following processes might be involved

$$Ru(NH_3)_6^{3+} + e^- \rightleftharpoons Ru(NH_3)_6^{2+} \tag{14}$$

$$\text{glucose} + O_2 \rightarrow \text{glucolactone} + H_2O_2 \tag{15}$$

$$Ru(NH_3)_6^{2+} + \frac{1}{2}H_2O_2 + H^+ \rightarrow Ru(NH_3)_6^{3+} + H_2O \tag{16}$$

For process (16), control experiments showed that ITO|TC exhibited insignificant effects on the reduction of H_2O_2 at pH 7 as $Ru(NH_3)_6^{3+}$ was excluded (Supporting Information, Figure S8). The TC sites on ITO|TC|GOx are less likely responsible for the transduction of H_2O_2, and more likely, functioning as microconductors to facilitate electrons to flow between the electrode and $Ru(NH_3)_6^{3+}$. According to eq 12, we calculated the pseudofirst-order reaction rate constant (k') for process (16). Provided that the diffusion coefficient of $Ru(NH_3)_6^{3+}$ (D) is 10^{-6} cm^2 s^{-1}, the value was calculated to be 8 cm^3 mol^{-1} s^{-1} at pH 7, close to the result obtained by substituting H_2O_2 for glucose under nitrogen (10 cm^3 mol^{-1} s^{-1}). These results indicate the glucose transduction at ITO|TC|GOx is nearly complete, proving that the function of GOx is not affected as adsorbed on ITO|TC. We have also characterized other phenothiazine molecules such as methylene blue and toluidine blue O for their potential in this aspect. Although their behavior was not as promising as TC, phenothiazine compounds appear to be potential molecular glues for protein immobilization.

In summary, phenothiazine compounds, such as thionine chloride, demonstrate a unique affinity for proteins. A variety of proteins including oxidase, dehydrogenase, iron-storage protein and DNA can thus be immobilized on solid surfaces like ITO. The affinity is ∼0.2 μN in strength, equivalent to 10^2

C−C single bonds. Although the strength is significant, TC appears not to interfere with the charge transport in the adsorbed proteins. Phenothiazine molecules thus prove as potential molecular adhesives for protein immobilization.

Acknowledgment. We acknowledge financial support from the National Science Council, Republic of China (Grant No. NSC 96-2113-M-003-MY3).

Supporting Information Available: Additional figures. This material is available free of charge via the Internet at http://pubs.acs.org.

References and Notes

(1) Gray, H. B.; Winkler, J. R. *Annu. Rev. Biochem.* **1996**, *65*, 537.
(2) Aviram, A.; Ratner, M. A. *Chem. Phys. Lett.* **1974**, *29*, 277.
(3) Simmons, J. G. *J. Appl. Phys.* **1963**, *34*, 1793.
(4) Rinaldi, R.; Biasco, A.; Maruccio, G.; Arima, V.; Visconti, P.; Cingolani, R.; Facci, P.; De Rienzo, F.; Di Felice, R.; Molinari, E.; Verbeet, M. Ph.; Canters, G. W. *Appl. Phys. Lett.* **2003**, *82*, 472.
(5) Cavalcanti, A.; Shirinzadeh, B.; Zhang, M.; Kretly, L. C. *Sensors* **2008**, *8*, 2932.
(6) Yang, T.; Jung, S.-y.; Mao, H.; Cremer, P. S. *Anal. Chem.* **2001**, *73*, 165.
(7) Giese, B.; Amaudrut, J.; Kohler, A. K.; Spormann, M.; Wessely, S. *Nature* **2001**, *412*, 318.
(8) Takada, T.; Kawai, K.; Fujitsuka, M.; Majima, T. *Proc. Natl. Acad. Sci. U.S.A.* **2004**, *101*, 14002.
(9) Drummond, T. G.; Hill, M. G.; Barton, J. K. *J. Am. Chem. Soc.* **2004**, *126*, 15010.
(10) Takada, T.; Takeda, Y.; Fujitsuka, M.; Majima, T. *J. Am. Chem. Soc.* **2009**, *131*, 6656.
(11) Reiss, B. D.; Hanson, D. K.; Firestone, M. A. *Biotechnol. Prog.* **2007**, *23*, 985.
(12) Cohen, H.; Nogues, C.; Naaman, R.; Porath, D. *Proc. Natl. Acad. Sci. U.S.A.* **2005**, *102*, 11589.
(13) Cui, J. D.; Primak, A.; Zarate, X.; Tomfohr, J.; Sankey, O. F.; Moore, A. L.; Moore, T. A.; Gust, D.; Harris, G.; Lindsay, S. M. *Science* **2001**, *294*, 571.
(14) Bradley, K.; Davis, A.; Gabriel, J. C. P.; Gruner, G. *Nano Lett.* **2005**, *5*, 841.
(15) Vaseasha, A.; Dimov-Malinovska, D. *Sci. Technol. Adv. Mater.* **2005**, *6*, 312.
(16) Zhao, J. W.; Davis, J. J.; Sansom, M. S. P.; Hung, A. *J. Am. Chem. Soc.* **2004**, *126*, 5601.
(17) Xu, D. G.; Watt, G. D.; Harb, J. N.; Davis, R. C. *Nano Lett.* **2005**, *5*, 571.
(18) Andolfi, L.; Bizzarri, A. R.; Cannistraro, S. *Appl. Phys. Lett.* **2006**, *89*, 183125.
(19) Zhang, Y.; Sheng, S.; Shao, Z. *Biophys. J.* **1996**, *71*, 2168.
(20) Tan, Y. H.; Liu, M.; Nolting, B.; Go, J. G.; Gervay-Hague, J.; Liu, G.-Y. *ACS Nano* **2008**, *2*, 2374.
(21) Okuro, K.; Kinbara, K.; Tsumoto, K.; Ishii, N.; Aida, T. *J. Am. Chem. Soc.* **2009**, *131*, 1626.
(22) Wu, S.-W.; Huang, H.-Y.; Guo, Y. C.; Wang, C. M. *J. Phys. Chem. C* **2008**, *112*, 9370.
(23) Libertino, S.; Giannazzo, F.; Aiello, V.; Scandurra, A.; Sinatra, F.; Renis, M.; Fichera, M. *Langmuir* **2008**, *24*, 1965.
(24) Muguruma, H.; Kase, Y.; Uehara, H. *Anal. Chem.* **2005**, *77*, 6557.
(25) Guiseppi-Elie, A.; Lei, C.; Baughman, R. H. *Nanotechnology* **2002**, *13*, 559.
(26) Alamarguy, D.; Benedetto, A.; Balog, M.; Noël, S.; Viel, P.; Le Derf, F.; Houze, F.; Sallé, M.; Palacin, S. *Surf. Interface Anal.* **2008**, *40*, 802.
(27) Pyon, M.-S.; Cherry, R. J.; Bjornsen, A. J.; Zapien, D. C. *Langmuir* **1999**, *15*, 7040.
(28) Sung, W. J.; Bae, Y. H. *Sens. Actuators, B* **2006**, *114*, 164.
(29) Blanch, M.; Legaz, M.-E.; Vicente, C. *Microbiol. Res.* **2008**, *163*, 362.
(30) Oubrie, A.; Rozeboom, H. J.; Dijkstra, B. W. *Proc. Natl. Acad. Sci. U.S.A.* **1999**, *96*, 11787.
(31) Foxon, S. P.; Phillips, T.; Gill, M. R.; Towrie, M.; Parker, A. W.; Webb, M.; Thomas, J. A. *Angew. Chem., Int. Ed.* **2007**, *46*, 3686.
(32) Persson, B. A.; Jönsson, B.; Lund, M. *J. Phys. Chem. B* **2009**, *113*, 10459.
(33) Grandbois, M.; Beyer, M.; Rief, M.; Clausen-Schaumann, H.; Gaub, H. E. *Science* **1999**, *283*, 1727.
(34) Sharma, L. B. *Metal-Semiconductor Schottky Barrier Junctions and Their Applications*; Plenum Press: New York, 1984.
(35) Porath, D.; Bezryadin, A.; De Vries, S.; Dekker, C. *Nature* **2000**, *403*, 635.
(36) Ratikin, A.; Aich, P.; Papadopoulos, C.; Kobzar, Y.; Wedeneev, A. S.; Lee, J. S.; Xu, J. M. *Phys. Rev. Lett.* **2001**, *86*, 3670.
(37) Ratner, M. A.; Davis, B.; Kemp, M.; Mujica, V.; Roitberg, A.; Yaliraki, S. *Ann. N.Y. Acad. Sci.* **1998**, *852*, 22.
(38) Good, R. H. Jr.; Muller, E. W. *Handbuch der Physik*; Springer-Verlag: Berlin, 1956; Vol. XXI, p 176.
(39) Casuso, I.; Fumagalli, L.; Samitier, J.; Padrós, E.; Reggiani, L.; Akimov, V.; Gomila, G. *Nanotechnology* **2007**, *18*, 465503.
(40) Lewis, F. D.; Liu, X.; Miller, S. E.; Hayes, R. T.; Wasielewski, M. *Nature* **2000**, *406*, 51.
(41) Nayak, A.; Suresh, K. A. *Phys. Rev. E* **2008**, *78*, 021606.
(42) Xu, B.; Zhang, P.; Li, X.; Tao, N. *Nano Lett.* **2004**, *4*, 1105.
(43) Kushimerick, J. G.; Whitaker, C. M.; Pollack, S. K.; Schull, T. L.; Shashidhar, R. *Nanotechnology* **2004**, *15*, S489.
(44) Kushimerick, J. G.; Pollack, S. K.; Yang, J. C.; Naciri, J.; Holt, D. B.; Ratner, M A.; Shashidhar, R. *Ann. N.Y. Acad. Sci.* **2003**, *1006*, 277.
(45) Holmlin, R. E.; Haag, R.; Chabinyc, M. L.; Ismagilov, R. F.; Cohen, A. E.; Terfort, A.; Rampi, M. A.; Whitesides, G. M. *J. Am. Chem. Soc.* **2001**, *123*, 5075.
(46) Wold, D. J.; Haag, R.; Rampi, M. A.; Frisbie, C. D. *J. Phys. Chem. B* **2002**, *106*, 2813.
(47) Reed, M. A.; Zhou, C.; Muller, C. J.; Burgin, T. P. *Science* **1997**, *278*, 252.
(48) Wold, D. J.; Frisbie, C. D. *J. Am. Chem. Soc.* **2000**, *122*, 1970.
(49) Murphy, C. J.; Arkin, M. R.; Jenkins, Y.; Ghatlia, N. D.; Bossmann, S. H.; Turro, N. J.; Barton, J. K. *Science* **1993**, *262*, 1025.
(50) Dandliker, P. J.; Holmlin, R. E.; Barton, J. K. *Science* **1997**, *275*, 1465.
(51) Saito, I.; Nakamura, T.; Nakatani, K.; Yoshioka, Y.; Yamakuchi, K.; Sugiyama, H. *J. Am. Chem. Soc.* **1998**, *120*, 12686.
(52) Steenken, S.; Jovanovic, S. V. *J. Am. Chem. Soc.* **1997**, *119*, 617.
(53) Seidel, C. A. M.; Schulz, A.; Sauer, M. H. M. *J. Phys. Chem.* **1996**, *100*, 5541.
(54) Levine, R. L.; Moskovitz, J.; Stadtman, E. R. *IUBMB Life* **2000**, *50*, 301.
(55) Moskovitz, J.; Bar-Noy, S.; Williams, W. M.; Requena, J.; Berlett, B. S.; Stadtman, E. R. *Proc. Natl. Acad. Sci. U.S.A.* **2001**, *98*, 12920.
(56) Roy, S.; Goedecker, S.; Field, M. J.; Penev, E. *J. Phys. Chem. B* **2009**, *113*, 7315.

JP9119099